# NON-ADIABATIC UNDER-EXPANDED JET THEORY FOR BLOWDOWN AND FIRE RESISTANCE RATING OF HYDROGEN TANK

**Dadashzadeh, M., Makarov, D., Kashkarov, S. and Molkov, V.**
**[1] Ulster University, Shore Road, Newtownabbey, BT37 0QB, UK, s.dadashzadeh@ulster.ac.uk**

## ABSTRACT

The European Regulations on type-approval of hydrogen vehicles require thermally-activated pressure relief device (TPRD) to be installed on hydrogen onboard storage tanks to release its content in a fire event to prevent its catastrophic rupture. The aim of this study is to develop a model for design of an inherently safer system TPRD-storage tank. Parameters of tank materials and hydrogen, external heat flux from the fire to the tank wall, TPRD diameter, time to initiate TPRD are input parameters of the model. The energy conservation equation and real gas equation of state are employed to describe the dynamic behaviour of the system. The under-expanded jet theory developed previously for adiabatic release from a storage tank is applied here to non-adiabatic blowdown of a tank in a fire. Unsteady heat transfer equation is used to calculate heat conduction through the tank wall. It includes the decomposition of the wall material due to high heat flux. The convective heat transfer between tank wall and hydrogen is modelled through the dimensionless Nusselt number correlations. The model is validated against two types of experiments, i.e. realistic (non-adiabatic) blowdown of high-pressure storage tank and failure of a tank without TPRD in a fire. The model is confirmed to be time efficient for computations and accurately predicts the dynamic pressure and temperature of the gas inside the tank, temperature profile within the tank wall, time to tank rupture in a fire and the blowdown time.

## NOMENCLATURE

| Symbol | Parameter | Unit |
|---|---|---|
| $A_{int}$ | Internal surface of tank | $m^2$ |
| $b$ | Co-volume constant of gas in Abel-Noble equation | $m^3/kg$ |
| $C_D$ | Discharge coefficient | - |
| $c_{p,air}$ | Specific heat capacity of air | J/kg/K |
| $c_{p,g}$ | Specific heat capacity of gas inside tank at constant pressure | J/kg/K |
| $c_{pw}$ | Specific heat capacity of tank wall material (carbon fibre reinforced polymer (CFRP): $c_{p\ wall\ (CFRP)}$; liner: $c_{p\ wall\ (liner)}$) | J/kg/K |
| $D_{ext}$ | External diameter of tank | m |
| $D_{int}$ | Internal diameter of tank | m |
| $D_2$ | Diameter of orifice (real nozzle) | m |
| $D_3$ | Diameter of notional nozzle | m |
| $g$ | Acceleration of gravity | $m/s^2$ |
| $H_d$ | Latent heat due to the melting of resin | J/kg |
| $h_{out}$ | Enthalpy going out of the tank | J/kg |
| $k_{ext}$ | Heat transfer coefficient at the external surface of wall | $W/m^2/K$ |
| $k_{int}$ | Heat transfer coefficient at the internal surface of wall | $W/m^2/K$ |
| $\dot{m}$ | Entrainment mass flow rate | Kg/s |
| $m_1$ | Mass of the gas in tank | kg |
| $m_1^0$ | Initial mass of the gas in tank | kg |
| $n$ | Control volume number | - |
| $Nu_{Din}$ | Nusselt number inside tank | - |
| $P_{amb}$ | Ambient pressure | Pa |
| $P_1$ | Pressure inside tank | Pa |
| $P_2$ | Pressure at orifice | Pa |
| $P_1^0$ | Initial pressure inside tank | Pa |

| | | |
|---|---|---|
| $Pr_{air}$ | Prandtl number of air | - |
| $Q$ | Heat into a system due from the surroundings | J |
| $Ra_{Din}$ | Rayleigh number of gas inside tank | - |
| $R_g$ | Hydrogen gas constant | $m^2/s^2/K$ |
| $S$ | Source term | $J/m^3/s$ |
| $T_{amb}$ | Ambient temperature | K |
| $T_1$ | Temperature of gas inside tank | K |
| $T_{w(ext)}$ | Temperature of the external surface of tank | K |
| $T_{w(int)}$ | Temperature of the internal surface of tank | K |
| $T_2$ | Temperature of gas at orifice | K |
| $T_3$ | Temperature of gas at notional nozzle | K |
| $T_1^0$ | Initial temperature of gas inside tank | K |
| $T_{melt1}$ | Temperature of initiation of resin decomposition | K |
| $T_{melt2}$ | Temperature of termination of resin decomposition | K |
| $T_{w(n)}$ | Temperature of wall at the grid-point "n" | K |
| $T_w$ | Temperature of wall | K |
| $T_w^0$ | Initial temperature of wall | K |
| $t$ | Time | s |
| $u_{air}$ | Velocity of surrounding air | m/s |
| $u_2$ | Velocity at orifice | m/s |
| $u_3$ | Velocity at notional nozzle | m/s |
| $U$ | Total internal energy of gas inside tank | J |
| $V$ | Volume of tank | $m^3$ |
| $\lambda_g$ | Thermal conductivity of gas | W/m/K |
| $\mu_g$ | Dynamic viscosity of gas | Pa·s |
| $\mu_{air}$ | Viscosity of air | Pa·s |
| $\lambda_{air}$ | Thermal conductivity of ambience | W/m/K |
| $\rho_{air}$ | Density of air | $kg/m^3$ |
| $\lambda_w$ | Thermal conductivity of tank wall (CFRP: $\lambda_{wall\ (CFRP)}$; liner: $\lambda_{wall\ (liner)}$) | W/m/K |
| $\rho_1^0$ | Initial density of the gas inside the tank | $kg/m^3$ |
| $\rho_1$ | Density of gas inside tank | $kg/m^3$ |
| $\rho_2$ | Density of gas at orifice | $kg/m^3$ |
| $\rho_3$ | Density of gas at notional nozzle | $kg/m^3$ |
| $\rho_w$ | Density of tank wall (CFRP: $\rho_{wall\ (CFRP)}$; liner: $\rho_{wall\ (liner)}$) | $kg/m^3$ |
| $\beta$ | Thermal expansion coefficient of gas inside tank | $K^{-1}$ |
| $\beta_d$ | Decomposition fraction | - |
| $\gamma$ | Ratio of the specific heats | - |

## 1.0 INTRODUCTION

Hydrogen is stored onboard in composite tanks at nominal working pressure of 35 MPa (buses) to 70 MPa (cars). When exposed to a fire the external side of the tank wall starts to degrade and tank gradually loses its load bearing ability over the time. Due to heat transfer through the tank wall temperature and pressure inside the tank start to grow. Eventually, when the degradation temperature front reaches a certain thickness of the tank wall where it meets the load bearing thickness of the wall, tank rupture occurs. This is accompanied by catastrophic consequences, i.e. devastating blast wave, fireball and projectiles [1]. The fire resistance rating (FRR), i.e. time span from a fire start to tank rupture in the absence of thermally-activated pressure relief device (TPRD) mimicking its failure to operate or its blockage in an accident, of currently used tanks is about 6-12 min [2], [3]. The

quantitative risk assessment [4] demonstrated that composite hydrogen storage tanks with FRR=6-12 min have a risk of human life loss in an road accident escalating to a fire and consequently the tank rupture of $3.14 \cdot 10^{-3}$ fatality/vehicle/year on London roads. This is two and half orders of magnitude above the acceptable level of risk of $10^{-5}$. The cost associated with loss of life in the accident in this case is 4.03M £/accident [4]. The European Regulations on type-approval of hydrogen vehicles require TPRD to be installed on hydrogen onboard tanks to release its content in a fire event and therefore prevent the catastrophic consequences of tank rupture. When a blowdown of hydrogen through TPRD is initiated, temperature inside the tank decreases due to gas expansion. The heat transfer through the tank wall and the wall degradation are affected by two competing processes: the increase of wall temperature due to heat flux from the fire, and the decrease of the wall temperature because of the drop of gas temperature inside the tank. Thus, the wall degradation front propagation slows down in conditions of blowdown compared to the case of closed vessel.

Inherently safer design of a tank-TPRD system is a challenging task with various parameters and processes involved, including tank volume, storage pressure, TPRD release diameter, TPRD initiating time, conductive heat transfer through the wall, convective heat transfer from the fire to the wall and from the wall to the gas inside the tank, wall material degradation due to the fire, etc. Experimental parametric study of these phenomena is an expensive task if possible at all. Computational fluid dynamics (CFD) is an alternative contemporary method to essentially decrease or even avoid the expensive experiments. However, CFD simulations are not time efficient [5].

The present study aims at development of the physical model for the inherently safer design of a pressurised tank-TPRD system. The model accounts for the conductive heat transfer through the tank wall caused by the convective heat transfer at the external side of the wall (either ambient conditions or fire) and the conductive heat transfer at the internal side of the tank wall between the gas and the wall. The TPRD release orifice size and its activation time are taken into consideration. The model predicts accurately pressure and temperature dynamics inside the tank during blowdown and the blowdown time. It predicts accurately as well the fire resistance rating of the tank, i.e. time to rupture of the tank in a fire.

## 2.0 PHYSICAL MODEL

The described below non-adiabatic blowdown model calculates pressure and temperature dynamics inside a tank for different conditions. The under-expanded jet theory [6] is used to calculate the gas parameters at the TPRD exit and at the notional nozzle exit. Figure 1 shows schematically different parts of a tank used in this study. Conductive heat transfer through the tank wall is calculated by exploiting one dimensional unsteady heat transfer equation using the finite-difference method [7]. The decomposition of the composite tank wall material (resin degradation) when temperature exceeds the decomposition value is modelled as [8]–[12]. To calculate the heat transfer coefficient for the natural and forced convection, Nusselt number correlations are applied [13].

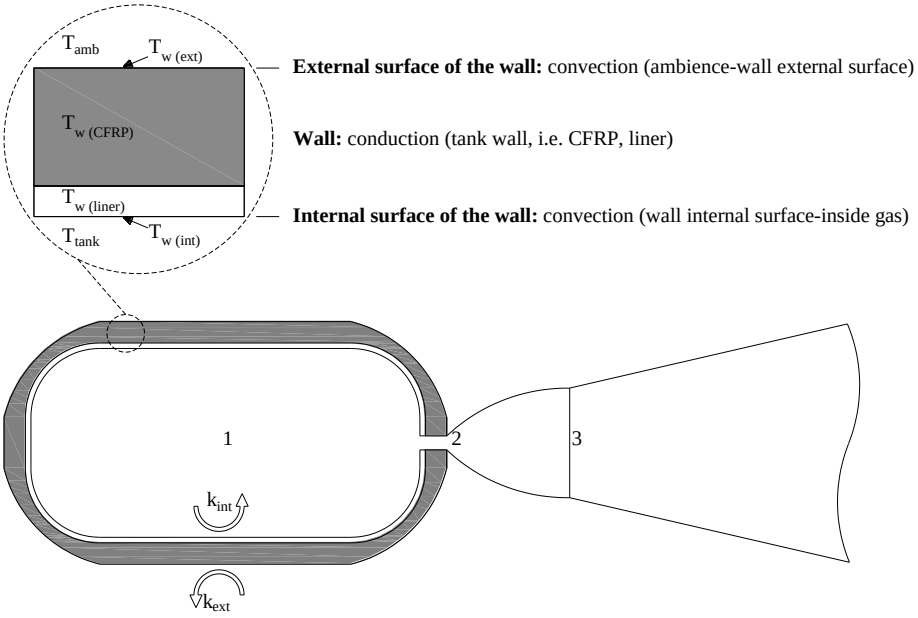


Figure 1. Schematic diagram of a pressurised tank: (1) internal tank space with gas, (2) actual nozzle exit of TPRD, (3) notional nozzle exit.

Hydrogen parameters are related through Abel-Noble real gas equation of state (EOS) [14]

$$P_1 = Z\rho_1 R_{H_2} T_1, \tag{1}$$

where $Z = 1/(1 - b\rho_1)$ is the compressibility factor, $P_1$, $\rho_1$ and $T_1$ are the pressure, the gas density and the gas temperature inside the tank respectively.

The first law of thermodynamic is used to bring together the rate of change of internal energy of hydrogen in the tank, the rate of heat transfer to/from hydrogen through the tank wall, composed of a composite polymer and a liner with different thermodynamic parameters, and the rate of enthalpy going out of the tank by hydrogen outflow

$$\frac{dU}{dt} = \frac{dQ}{dt} - h_{out}\frac{dm}{dt}, \tag{2}$$

where the enthalpy of the gas going out of the tank is $h_{out} = c_{p,g}T_1 + bP_1$.

The internal energy of real gas is calculated as [16]

$$U = \frac{P_1(V - m_1 b)}{\gamma - 1}, \tag{3}$$

The rate of heat transfer by convection through the internal tank surface wall is modelled as [17]

$$\frac{\mathrm{d}Q}{\mathrm{d}t} = k_{int}A_{int}\left(T_{w(int)} - T_1\right). \tag{4}$$

The value of heat transfer coefficient at internal tank surface $k_{int}$ is calculated as a function of Nusselt number, internal tank diameter, and the gas thermal conductivity which is interpolated for different pressure and temperature from [18], respectively as

$$k_{int} = \frac{\lambda_g \times Nu_{Din}}{D_{int}}. \quad (5)$$

Natural convection Nusselt number, $Nu_{Din}$, is calculated by the empirical equation [13]

$$Nu_{Din} = 0.104 \times \left( \frac{g\beta \left| T_1 - T_{w(int)} \right| c_{p,g} (\rho_1)^2 D_{int}^3}{\mu_g \lambda_g} \right)^{0.352}. \quad (6)$$

Differentiating Eq. (3) and considering the rate of heat transfer, defined by Eq. (4), the differential equation for calculation of hydrogen pressure in the tank, $P_1$, can be obtained from Eq. (2)

$$\frac{\mathrm{d}P_1}{\mathrm{d}t} = \frac{\frac{dm}{dt} \cdot \left( \frac{P_1}{\gamma - 1} - c_{p,g} \cdot T_1 \right) + k_{int} A_{int} (T_{w(int)} - T_1)}{\frac{V - m_1 \cdot b}{\gamma - 1}}. \quad (7)$$

The density is calculated as $\rho_1 = \frac{m_1}{V}$ and it is followed by using Eq. (24) [14] to calculate the temperature of the hydrogen inside the tank in the assumption of uniformity of hydrogen temperature throughout the tank ($T_1$)

$$T_1 = \frac{P_1 (1 - b\rho_1)}{\rho_1 R_{H_2}}. \quad (8)$$

The under-expanded jet theory [6], [15] is used for the calculation of parameters at the actual nozzle exit and notional nozzle exit. To find the gas density at the actual (TPRD) nozzle exit, $\rho_2$, the following transcendental equation of isentropic expansion [15] is included into the system of equations

$$\left[ \frac{\rho_1}{1 - b\rho_1} \right]^{\gamma} = \left[ \frac{\rho_2}{1 - b\rho_2} \right]^{\gamma} \cdot \left[ 1 + \left( \frac{\gamma - 1}{2(1 - b\rho_2)^2} \right) \right]^{\gamma/\gamma - 1}. \quad (9)$$

The temperature of the gas at the TPRD exit is calculated by using the energy conservation equation for gas inside the tank and at the actual nozzle exit in the form [15]

$$\frac{T_1}{T_2} = 1 + \frac{\gamma - 1}{2(1 - b\rho_2)^2}. \quad (10)$$

Abel-Noble EOS [14] is used for the calculation of pressure at the actual nozzle exit

$$P_2 = \frac{\rho_2 R_g T_2}{1 - b\rho_2}. \quad (11)$$

Considering the chocked flow at the orifice, the gas velocity is assumed to be equal to the local sound velocity [14], [15], hence the flow velocity from the actual nozzle (TPRD) exit is

$$u_2 = \frac{\left( \gamma R_g T_2 \right)^{0.5}}{1 - b\rho_2}. \quad (12)$$

The gas velocity at the notional nozzle is assumed to be equal to the local sound velocity, hence the energy conservation equation in the form of [6], [15] is employed to calculate the temperature at the notional nozzle

$$T_3 = \frac{2T_2}{\gamma + 1} + \frac{(\gamma - 1)}{(\gamma + 1)} \cdot \frac{P_2}{\rho_2 (1 - b\rho_2) R_g}. \quad (13)$$

Considering the gas pressure at the notional nozzle to be equal to the ambient pressure ($P_{amb}$), Abel-Noble EOS [14] is employed to calculate the gas density at the notional nozzle

$$\rho_3 = \frac{P_{amb}}{P_{amb}b + R_g T_3}. \tag{14}$$

The gas velocity at the notional nozzle is then calculated by the expression of local sound velocity [6], [15]

$$u_3 = \frac{\left(\gamma R_g T_3\right)^{0.5}}{1 - b\rho_3}. \tag{15}$$

The continuity equation between the actual and the notional nozzle is used to calculate the diameter of the notional nozzle followed by the equation for mass flow rate, $\dot{m} = \frac{dm}{dt}$,

$$D_3 = D_2 \sqrt{C_D \frac{\rho_2 u_2}{\rho_3 u_3}}, \tag{16}$$

$$\dot{m} = \frac{\rho_3 u_3 \pi (D_3)^2}{4}, \tag{17}$$

where $D_2$ is the actual nozzle diameter, $D_3$ is the notional nozzle diameter and $C_D$ is the discharge coefficient, which is introduced into the model for accounting for possible friction and minor losses in the TPRD. At each time step, ṁ is updated and is used as an input to Eq. (7).

The model solves the unsteady heat conduction equation through the tank wall which can be found elsewhere [7]

$$\rho_w c_{pw} \frac{dT_w}{dt} = \frac{d}{dx}\left(\lambda_w \frac{dT_w}{dx}\right) + S. \tag{18}$$

The heat of resin degradation, i.e. energy required to decompose the resin, is introduced in a form of the energy sink term, *S*. This heat is consumed within the range of resin decomposition temperatures known from literature [19]–[23]. The source term $S$ in Eq. (18) is implemented following [8]–[12]

$$S = -\rho_w \beta_d \frac{dH_d}{dt}, \tag{19}$$

where $\beta_d$ is the decomposition fraction and $H_d$ is the latent heat due to the melting of resin. The value of fraction $\beta_d$ changes between 0 and 1 in each control volume of the wall, as governed by the following conditions

$$\begin{cases} \beta_d = 0 & \text{if } T_{w(n)} < T_{melt1} \text{ or } T_{w(n)} > T_{melt2} \\ \beta_d = 1 & \text{if } T_{melt1} \le T_{w(n)} \le T_{melt2} \end{cases},$$

where $T_{melt1}$ and $T_{melt2}$ are the initiation temperature and termination temperature for the decomposition of resin, respectively.

The fraction $\beta_d$ turns 1 as the temperature of a control volume is in the range of $T_{melt1}$ to $T_{melt2}$. Therefore, the energy (latent heat) is sunk in this control volume. The rate of the latent heat change ($\frac{dH_d}{dt}$) over decomposition temperature range is presented in Fig. 2 and expressed in the following form

$$\frac{dH_d}{dt} = \frac{dT_w}{dt} \cdot \frac{H_d}{T_{melt2} - T_{melt1}}. \quad (20)$$

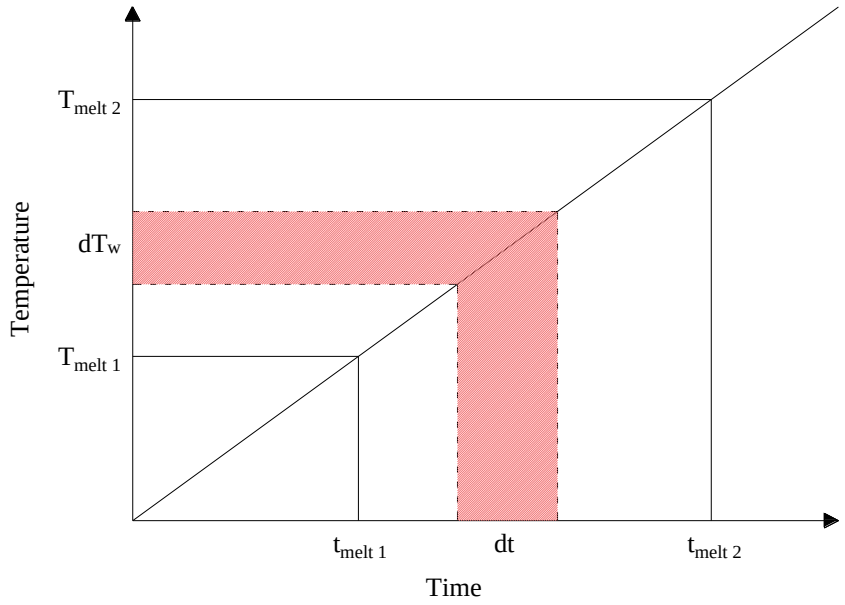


Figure 2. Schematic diagram of latent heat linearization over the decomposition temperature range.

The conservation of energy requires the equality of the convective heat flux between gas and the wall to the conductive heat flux at the wall boundary. Thus, boundary conditions at internal and external surfaces of the tank are defined by Eq. (21) and Eq. (22) respectively

$$q^{"}_{conduction}\ \ (internal) = q^{"}_{convection} - \lambda_w \frac{dT_{w\,(n)}}{dx}\Big|_{n=int} = k_{int}\left(T_1 - T_{w\,(int)}\right), \quad (21)$$

$$q^{"}_{conduction}\ \ (external) = q^{"}_{convection} \Rightarrow -\lambda_w \frac{dT_{w\,(n)}}{dx}\Big|_{n=ext} = k_{ext}\left(T_{w\,(ext)} - T_{amb}\right). \quad (22)$$

It was observed previously and published elsewhere [7,21] that the external convective heat transfer coefficient, $k_{ext}$, does not have a significant effect on heat transfer. For the model validation of the blowdown phenomenon without a fire, the value of $k_{ext}$ is then accepted to be 6 W/m$^2$/K in our study following [21]. For the model validation of the case of tank rupture in a fire without blowdown (closed tank without activated TPRD), the heat flux dynamics on the dome part of the tank was extracted from the full 3D CFD simulation and it was implemented in the model as a function of time

$$q" = -5 \cdot 10^{-10}t^5 + 1 \cdot 10^{-6}t^4 - 0.0013t^3 + 0.6489t^2 - 185.73t + 54166. \quad (23)$$

For the case of tank rupture in a fire without blowdown problem, Eq. (22) is simplified in the form of

$$q^{"}_{conduction}\ \ (external) = q^{"}_{convection} \Rightarrow \quad -\lambda_w \frac{dT_{w\,(n)}}{dx}\Big|_{n=ext} = q". \quad (24)$$

The system of equations is solved iteratively. Before the start of calculations, the mass flow rate is $\dot{m}^0$ =0 kg/s. Initial conditions (iteration number $i = 0$) are

$$\rho_1^0 = \frac{P_1^0}{P_1^0 \cdot b + R_g \cdot T_1^0},$$

$$m_1^0 = V \cdot \rho_1^0,$$

$$Nu_{int}^{0} = 0.104 \times \left( \frac{g\beta \left| T_1^0 - T_{w(int)}^0 \right| c_{p,g} \left(\rho_1^0\right)^2 D_{int}^3}{\mu_g \lambda_g} \right)^{0.352},$$

$$k_{int\ natural}^{0} = \frac{\lambda_g \cdot Nu_{int\ natural}^{0}}{D_{int}}.$$

The model input parameters are presented in Table 1. The model can predict the dynamics of gas temperature and pressure inside the tank, the temperature profile within the load bearing wall and the liner, the blowdown time or the fire resistance rating (time to tank rupture in a fire).

Table 1. Input parameters, calculation procedure and output parameters.

| **Input parameters** | |
|---|---|
| $V$, $b$, $\gamma$, $T_{amb}$, $q"$, $T_1^0$, $T_w^0$, $P_1^0$, $A_{int}$, $\Delta x$, $\Delta t$, $R_g$, $\rho_{w(n)}$, $c_{p\,w(n)}$, $\lambda_w$, $k_{ext}$, $D_{int}$, $g$, $\beta$, $T_w^0$, $k_{int}^0$, $c_{p,g}$, $\mu_g$, $\lambda_g$, $\rho_1^0$, $m_1^0$ | |
| **Calculation procedures** | |
| **Step No.** | **Output parameters** |
| 1 | Hydrogen mass in tank, ($m_1^i = m_1^{i-1} + \left(\frac{dm}{dt}\right)\Delta t$) |
| 2 | Hydrogen density in tank, $\rho_1 = \frac{m_1}{V}$ |
| 3 | Pressure change (ramp) in tank ($\frac{dP_{tank}}{dt}$), Eq. (7) |
| 4 | Hydrogen pressure in tank ($P_1$), $P_1^i = P_1^{i-1} + \left(\frac{dP_1}{dt}\right)\Delta t$ |
| 5 | Hydrogen temperature in tank ($T_1$), Eq. (8) |
| 6 | Hydrogen density at orifice ($\rho_2$), Eq. (9) |
| 7 | Hydrogen temperature at orifice ($T_2$), Eq. (10) |
| 8 | Hydrogen pressure at orifice ($P_2$), Eq. (11) |
| 9 | Hydrogen velocity at orifice ($u_2$), Eq. (12) |
| 10 | Hydrogen temperature at notional nozzle ($T_3$), Eq. (13) |
| 11 | Hydrogen density at notional nozzle ($\rho_3$), Eq. (14) |
| 12 | Hydrogen velocity at notional nozzle ($u_3$), Eq. (15) |
| 13 | Diameter of notional nozzle ($D_3$), Eq. (16) |
| 14 | Mass flow rate ($\dot{m} = \frac{dm}{dt}$), Eq. (17) |
| 16 | Transient temperature within tank wall ($T_w$), Eq. (18) |
| 17 | Temperature at the wall internal surface ($T_{w\,(int)}$), Eq. (21) |
| 18 | Temperature at the wall external surface ($T_{w\,(ext)}$),<br>Eq. (22) in the case of blowdown with no fire;<br>Eq. (24) in the case of tank rupture in a fire |
| 20 | Heat transfer coefficient at the internal surface of the wall ($k_{int}$), Eq. (5) |
| 21 | Repeating steps 1 to 20 if $P_1/P_{amb}$ > 1.9. else simulation is stopped. |

## 3.0 THE MODEL VALIDATION

The model was validated against two experiments: blowdown of helium from 70 MPa storage tank without fire, and the failure of the hydrogen 70 MPa tank in a fire without blowdown.

### 3.1 Blowdown test

The validation experiment was carried out in the HYKA-HyJet research facility at Karlsruhe Institute of Technology (KIT). The impinging jet test platform was used with a high-pressure Type IV tank of volume 19 litres connected to a release nozzle with 1 mm diameter exit. The storage vessel was firstly filled in to 70 MPa by helium and then cooled down to a normal room temperature (293 K) before the

start of blowdown test. The tank characteristics are presented in Table 2. Temperature inside the tank was measured by a thermocouple installed in the middle of the tank. Pressure dynamics inside the tank was also measured during the blowdown test.

Table 2. Dimensions and properties of tank used in blowdown experiment.

| **Parameter** | **Value** | **Reference** |
|---|---|---|
| Type IV tank | | |
| Internal volume, L | 19 | [24] |
| Internal diameter, mm | 180 | [24] |
| External diameter, mm | 228 | [24] |
| External length, mm | 0.904 | [24] |
| **HDPE* liner** | | |
| Thickness, mm | 7 | [25] |
| Thermal conductivity, W/m/K | 0.385 | [26] |
| Specific heat capacity, J/kg/K | 1584 | [26] |
| Density, kg/m3 | 945 | [26] |
| **CFRP* structural layer** | | |
| Thickness, mm | 17 | [25] |
| Thermal conductivity, mm | 0.5 | [27] |
| Specific heat capacity, J/kg/K | 1020 | [27] |
| Density, kg/m3 | 1360 | [27] |

***** HDPE: high density polyethylene; AA: aluminium alloy; CFRP: carbon fibre reinforced polymer.

Table 3 shows input parameters used to perform the blowdown simulations for the described test using the model.

Table 3. Input parameters for the blowdown of helium test (70 MPa, 19 litre Type IV cylinder).

| **Parameter** | **Value** | **Reference** |
|---|---|---|
| $c_{p,g}$, J/kg/K | Interpolated function | [28] |
| $\lambda_g$, W/m/K | Interpolated function | [28] |
| $\beta$, 1/K | Interpolated function | [28] |
| $R_{He}$, Nm/kg/K | 2080 | [28] |
| $\gamma_g$ | 1.66 | [28] |
| b, $m^3/kg$ | $2.67 \cdot 10^{-3}$ | [29] |
| $M_g$, g/mol | 4.003 | [28] |
| g, $m/s^2$ | 9.81 | constant, model assumption |
| $T_{amb}$, K | 293 | model assumption |
| $P_{amb}$, Pa | $1.01 \cdot 10^5$ | model assumption |
| $T_1^0$, K | 293 | KIT experiment |
| $P_1^0$, Pa | $7.00 \cdot 10^7$ | KIT experiment |
| $\rho_1^0$, $kg/m^3$ | $8.80 \cdot 10^1$ | Eq. (29) |
| $m_1^0$, $kg/m^3$ | 1.67 | Eq. (30) |
| $\mu_{air}$, Pa·s | $1.98 \cdot 10^{-5}$ | [30] |
| $c_{p,air}$, J/kg/K | $1.01 \cdot 10^3$ | [30] |
| $\lambda_{air}$, W/m/K | $2.57 \cdot 10^{-2}$ | [30] |
| $\rho_{air}$, $kg/m^3$ | 1.21 | [30] |

Figure 3 demonstrates the measured and calculated pressure (Fig. 3a) and temperature (Fig. 3b) for both the adiabatic blowdown model [6] and the non-adiabatic blowdown model of this study. During the simulation for either the adiabatic blowdown model [6] and non-adiabatic blowdown model (this

study), the discharge coefficient $C_D$=0.9 is used here similar to [31], which corresponds to the best fit of calculated to experimental data. The simulated gas pressure with non-adiabatic blowdown model is in an excellent agreement with the experiment (Fig. 3a) and is more accurate compared to the adiabatic model. The non-adiabatic model performance for gas temperature inside the tank even more impressive (Fig. 3b), closely following the experimental temperature dynamics (within 6% deviation from measured values) which is quite opposite to monotonically decreasing temperature dynamics of the adiabatic blowdown model.

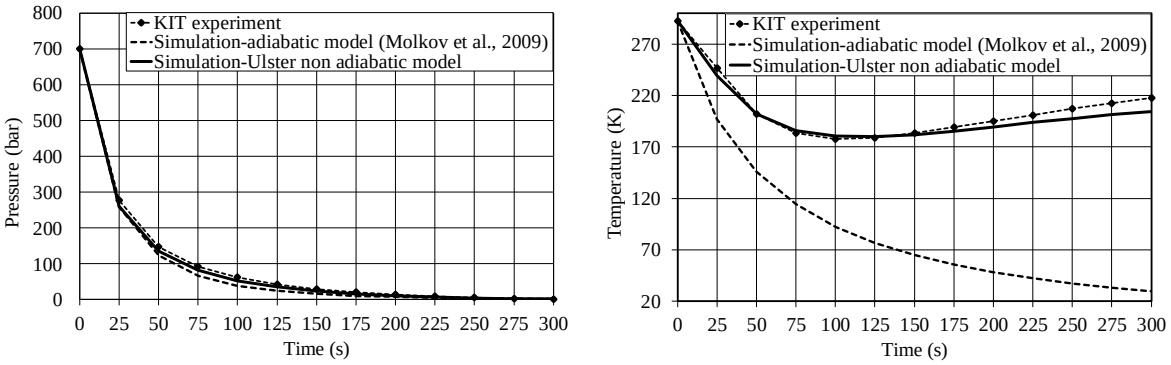


(a) (b)

Figure 3. Simulations versus experimental data for the adiabatic blowdown model [6] and the non-adiabatic blowdown model (this study): (a) pressure inside the tank; (b) gas temperature inside the tank.

### 3.2 Tank rupture in a fire test

The fire test with hydrogen tank was performed at KIT (Germany) using the HYKA-A2 facility in the framework of European project H2FC (www.h2fc.eu). The test was performed using 36 litre Type IV tank. The length and diameter of the tank were 0.910 m and 0.325 m respectively. The tank was filled in with hydrogen to the nominal working pressure (NWP) of 70 MPa. The main purpose of the test was to define the fire resistance rating, i.e. time to tank rupture when exposed to a fire. The premixed methane-air burner was used inside the large closed facility. To exclude hydrogen combustion after the tank rupture the surrounding atmosphere in the facility was filled in with nitrogen. The heat release rate of the fire was 170 kW. The details of the fire test, the installation configuration and the instrumentations provided fulfilment of the GTR#13 requirements [32] and are explained in [33]. Two tests with the same condition were performed in which the tank rupture occurred at 8 min and 3 s in Test 1 and 9 min 42 s in Test 2. The tank parameters and thermal properties are shown in Table 4.

Table 4. Dimensions and properties of tank used in tank failure in a fire experiment.

| **Parameter** | **Value** | **Reference** |
|---|---|---|
| **Type IV tank** | | |
| Internal volume, L | 36 | KIT experiment |
| Internal diameter, mm | 262 | KIT experiment |
| External diameter, mm | 325 | KIT experiment |
| External area, $m^2$ | 0.63 | KIT experiment |
| **HDPE liner** | | |
| Thickness, mm | 5.27 | [23] |
| Thermal conductivity, W/m/K | 0.4 @ 293 K<br>0.2 @ 423 K | [34] |
| Specific heat capacity, J/kg/K | 2000 @ 293 K<br>2600 @ 423 K | [34] |
| Density, $kg/m^3$ | 940 | [34] |

| Parameter | Value | Reference |
|---|---|---|
| **CFRP structural layer** | | |
| Thickness, mm | 22.26 | [23] |
| Thermal conductivity, W/m/K | Correlation | [25] |
| Specific heat capacity, J/kg/K | Correlation | [25] |
| Density, kg/m$^3$ | 1360 | [27] |
| Latent decomposition heat, J/kg | $3.50 \cdot 10^5$ | [35] |
| Decomposition temperature, K | 613-633 | [19]–[23] |

The GTR#13 requirement to the minimal burst pressure for the CFRP overwrapped Type IV tank is 2.25 times NWP, or greater (safety factor) whereas the design is maintained in a way it can withstand +/-10% of initial burst pressure [32]. Then the transient load bearing fraction of the tank wall thickness is $P_{current}/(2.25 \cdot NWP)$, where $P_{current}$ is the transient pressure inside the tank during the fire [33]. For a tank with NWP 70 MPa, this means that 1/2.25=0.44 fraction of the tank wall thickness is sufficient to withstand the pressure of 70 MPa. In fire conditions, temperature inside the tank and consequently the pressure grow, hence the fraction of the wall thickness that can keep the tank intact increases. The tank wall thickness fraction that can handle the pressure load whilst the composite resin is decomposed without tank rupture is: $1 - [P_{current}/(2.25 \cdot NWP)]$. Thus, the model calculates the time to rupture as the time during which the decomposition temperature of the resin (613 K) front reaches depth of the wall equal to $1 - [P_{current}/(2.25 \cdot NWP)]$. For the tank used in the test the rupture is expected at the dome part of the tank where the tank wall is thinner compared to the cylindrical part of the wall (Fig. 4).

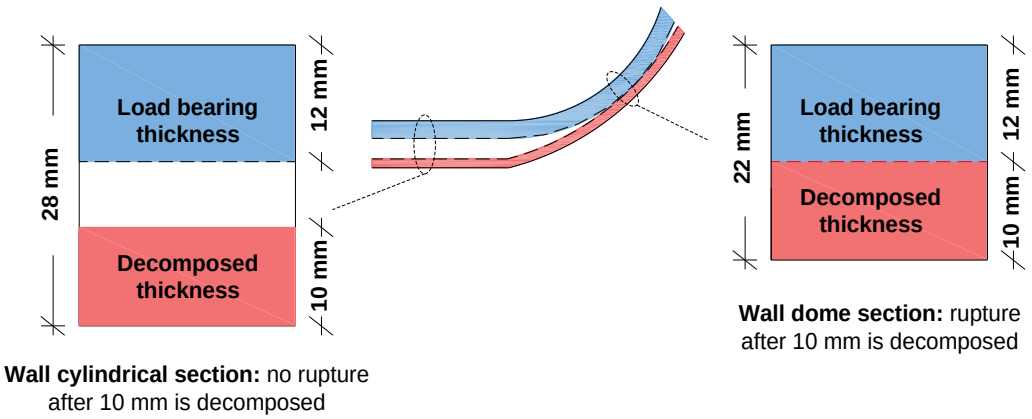


Figure 4. Tank wall thickness at the cylindrical and the dome section.

Table 5 presents the input parameter used in the model to reproduce experimental data.

Table 5. The model input parameters for the tank rupture in a fire test (70 MPa, 36 litre Type IV tank).

| Parameter | Value | Reference |
|---|---|---|
| $c_{p,g}$, J/kg/K | Interpolated function | [18] |
| $\lambda_g$, W/m/K | Interpolated function | [18] |
| $\beta$, 1/K | Interpolated function | [18] |
| $R_{H_2}$, Nm/kg/K | 4124.24 | [18] |
| $\gamma_{H_2}$ | 1.41 | [18] |
| b, m$^3$/kg | $7.69 \cdot 10^{-3}$ | [29] |
| $M_{H_2}$, g/mol | 2.016 | [18] |
| $T_{amb}$, K | 308 | Model assumption |
| $P_{amb}$, Pa | $1.01 \cdot 10^5$ | Model assumption |

| Parameter | Value | Reference |
|---|---|---|
| $T_1^0$, K | 308 | KIT experiment |
| $P_1^0$, Pa | $7.01 \cdot 10^7$ | KIT experiment |
| $\rho_1^0$, kg/m$^3$ | $3.87 \cdot 10^1$ | Eq. (29) |
| $m_1^0$, kg/m$^3$ | 1.39 | Eq. (30) |

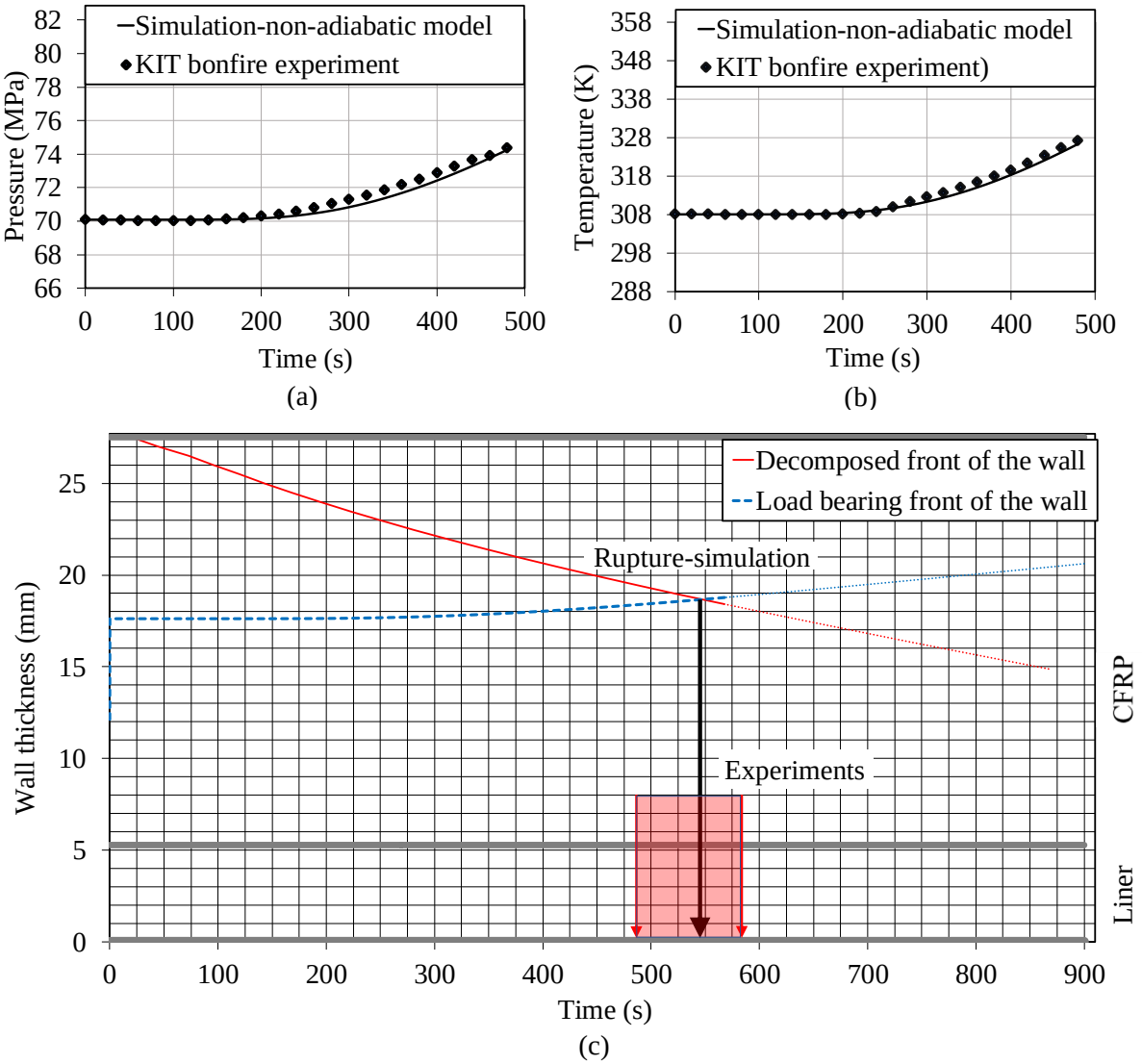


Figure 5. Comparison of model calculations with experimental data: (a) - pressure dynamics inside the tank; (b) temperature dynamics inside the tank; (c) time to tank rupture.

Figure 5 compares the simulated pressure dynamic inside the tank (Fig.5a), temperature dynamics inside the tank (Fig.5b) and the fire resistance rating, i.e. time to tank rupture in a fire (Fig. 5c). The calculated pressure and temperature are in an excellent agreement with the experimental measurements. Considering the described above tank rupture criteria in a fire the calculated by the model fire resistance rating (FRR) is 9 min 8 s. This is between two experimental values of FRR, i.e. 8 min 3 s for Test 1, and 9 min 42 s for Test 2. The physical model is thus confirmed to predict the time to tank rupture in a fire with acceptable accuracy (Fig. 5c).

## 4.0 CONCLUSIONS

The significance of this study is in the development of the non-adiabatic model that can be applied to different process involving high-pressure gas storage tanks, including but not limited to blowdown, tank rupture in a fire, combination of both, etc. The model accounts for all underlying physical phenomena and can be used for the inherently safer design of a system TPRD-storage tank or calculation of fire resistance rating of a tank with failed to operate or blocked during an accident TPRD. The model accurately predicts thermal behaviour of the gas and the tank wall during blowdown, in a fire conditions, etc.

The rigour of this study is in the model validation against experimental data on: the blowdown of 19 litres volume Type IV tank with the working pressure of 70 MPa filled in with helium and TPRD diameter of 1 mm; the fire test with 36 litres volume Type IV tank with the working pressure of 70 MPa filled in by hydrogen and without TPRD to determine its fire resistance rating needed by first responders to develop their intervention strategies and tactics. The predicted dynamic pressure and temperature of gas inside a tank were in excellent agreement with the experiment for both validation tests. The calculated fire resistance rating of the tank in a fire is 9 min 8 s. This is in the middle between FRR=8 min 3 s in KIT fire Test 1, and 9 min 42 s in Test 2.

The originality of this study is in: (1) the inclusion of convective and conductive heat and mass transfer to the non-adiabatic model of high-pressure composite vessel behaviour in different conditions of their use, including processes of blowdown and fire, and (2) the integration of the unique tank failure in a fire criterion into the physical model to accurately predict fire resistance rating.

The model is used in safety engineering as a tool for cost effective and time efficient design of an inherently safer tank-TPRD system and calculation of fire resistance rating of high-pressure tank for storage of compressed gas.

## ACKNOWLEDGEMENTS

The authors are grateful to UK Engineering and Physical Sciences Research Council (EPSRC) for funding through EPSRC SUPERGEN H2FC Hub (EP/J016454/1 and EP/P024807/1) and EPSRC SUPERGEN Challenge “Integrated safety strategies for onboard hydrogen storage” (EP/K021109/1) projects. This research is supported by the Project “HYLANTIC”–EAPA_204/2016 which is co-financed by the European Regional Development Fund in the framework of the Interreg Atlantic programme.

## REFERENCES

[1] S. Brennan and V. Molkov, “Safety assessment of unignited hydrogen discharge from onboard storage in garages with low levels of natural ventilation,” *Int. J. Hydrogen Energy*, vol. 38, no. 19, pp. 8159–8166, Jun. 2013.

[2] N. C. Weyandt, “Analysis of Induced Catastrophic Failure of a 5000 psig Type IV Hydrogen Cylinder,” La Canada, California, 2005.

[3] N. C. Weyandt, “Vehicle bonfire to induce catastrophic failure of a 5000-psig hydrogen cylinder installed on a typical SUV,” 2006.

[4] M. Dadashzadeh, S. Kashkarov, D. Makarov, and V. Molkov, “Risk assessment methodology for onboard hydrogen storage,” *Int. J. Hydrogen Energy*, vol. 43, pp. 6462–6475, 2018.

[5] T. Bourgeois, F. Ammouri, M. Weber, and C. Knapik, “Evaluating the temperature inside a tank during a filling with highly-pressurized gas,” *Int. J. Hydrogen Energy*, vol. 40, no. 35, pp. 11748–11755, Sep. 2015.

[6] V. Molkov, D. Makarov, and M. V. Bragin, “Physics and modelling of underexpanded jets and hydrogen dispersion in atmosphere,” *Phys. Extereme States Matter*, pp. 146–149, 2009.

[7] S. V. Patankar, *Numerical heat transfer and fluid flow (Series in computational methods in mechanics and thermal sciences)*. New York: McGRAW-HILL BOOK COMPANY, 1980.

[8] V. R. Voller, “A Heat Balance Integral Method for Estimating Practical Solidification Parameters,” *IMA J. Appl. Math.*, vol. 35, no. 2, pp. 223–232, Sep. 1985.

[9] V. R. Voller and C. Prakash, “A fixed grid numerical modelling methodology for convection-diffusion mushy region phase-change problems,” *Int. J. Heat Mass Transf.*, vol. 30, no. 8, pp. 1709–1719, Aug. 1987.

[10] V. R. Voller, “Development and application of a heat balance integral method for analysis of metallurgical solidification,” *Appl. Math. Model.*, vol. 13, no. 1, pp. 3–11, Jan. 1989.

[11] V. R. Voller, A. D. Brent, and C. Prakash, “Modelling the mushy region in a binary alloy,” *Appl. Math. Model.*, vol. 14, no. 6, pp. 320–326, Jun. 1990.

[12] S. Wang, A. Faghri, and T. L. Bergman, “A comprehensive numerical model for melting with natural convection,” *Int. J. Heat Mass Transf.*, vol. 53, no. 9–10, pp. 1986–2000, Apr. 2010.

[13] P. L. Woodfield, M. Monde, and T. Takano, “Heat tranfer charateristics for practical hydrogen vessels being filled at high pressure,” *J. Therm. Sci. Technol.*, vol. 3, pp. 241–253, 2008.

[14] I. Johnson, “The Noble-Abel equation of state: thermodynamic derivations for ballistics modelling,” 2005.

[15] V. Molkov, *Fundamentals of hydrogen safety engineering I*. bookboon.com, 2012.

[16] V. Molkov and S. Kashkarov, “Blast wave from a high-pressure gas tank rupture in a fire: Stand-alone and under-vehicle hydrogen tanks,” *Int. J. Hydrogen Energy*, vol. 40, no. 36, pp. 12581–12603, Sep. 2015.

[17] M. Monde, P. Woodfield, T. Takano, and M. Kosaka, “Estimation of temperature change in practical hydrogen pressure tanks being filled at high pressures of 35 and 70 MPa,” *Int. J. Hydrogen Energy*, vol. 37, no. 7, pp. 5723–5734, 2012.

[18] NIST, “Isothermal properties for hydrogen,” 2017. [Online]. Available: http://webbook.nist.gov/cgi/inchi?ID=C1333740&Mask=1#Thermo-Gas.

[19] C.-L. Chiang, R.-C. Chang, and Y.-C. Chiu, “Thermal stability and degradation kinetics of novel organic/inorganic epoxy hybrid containing nitrogen/silicon/phosphorus by sol–gel method,” *Thermochim. Acta*, vol. 453, no. 2, pp. 97–104, Feb. 2007.

[20] N. Régnier and S. Fontaine, “Determination of the Thermal Degradation Kinetic Parameters of Carbon Fibre Reinforced Epoxy Using TG,” *J. Therm. Anal. Calorim.*, vol. 64, no. 2, pp. 789–799, May 2001.

[21] W. Liu, R. J. Varley, and G. P. Simon, “Understanding the decomposition and fire performance processes in phosphorus and nanomodified high performance epoxy resins and composites,” *Polymer (Guildf).*, vol. 48, no. 8, pp. 2345–2354, Apr. 2007.

[22] P. T. Niranjana, H. Y. J., H. V., P. K., and I. P., “Thermal degradation of epoxy resin reinforced with polypropylene fibers,” *J. Appl. Polym. Sci.*, vol. 104, no. 1, pp. 500–503, Jan. 2007.

[23] S. Kashkarov, D. Makarov, and V. Molkov, “Model of 3D conjugate heat transfer and mechanism of compressed gas storage failure in a fire,” in *7th International Conference on Hydrogen Safety (ICHS)*, 2017.

[24] B. Acosta, P. Moretto, N. de Miguel, R. Ortiz, F. Harskamp, and C. Bonato, “JRC reference data from experiments of on-board hydrogen tanks fast filling,” *Int. J. Hydrogen Energy*, vol. 39, no. 35, pp. 20531–20537, Dec. 2014.

[25] S. Welch, R. Hadden, J. Hidalgo-Medina, and P. Pironi, “Thermal properties and thermal modelling of composite materials exposed to fires,” 2017.

[26] M. Monde and M. Kosaka, “Understanding of Thermal Characteristics of Fueling Hydrogen High Pressure Tanks and Governing Parameters,” *SAE Int. J. Altern. Powertrains*, vol. 2, no. 1, pp. 61–67, 2013.

[27] J. P. Hidalgo, P. Pironi, R. M. Haden, and S. Welch, “Effect of Thickness on the Ignition Behaviour of Carbon Fibre Composite Materials Used in High Pressure Vessels,” in *Eight International Seminar on Fire and Explosion Hazards (ISFEH8)*, 2016.

[28] NIST, “Isothermal properties for helium,” 2017. [Online]. Available: http://webbook.nist.gov/cgi/fluid.cgi?T=293&PLow=0&PHigh=70&PInc=&Applet=on&Digits=5&ID=C7440597&Action=Load&Type=IsoTherm&TUnit=K&PUnit=MPa&DUnit=mol%2Fl&HUnit=kJ%2Fmol&WUnit=m%2Fs&VisUnit=uPa*s&STUnit=N%2Fm&RefState=DEF.

[29] Chenoweth D.R., “Gas-transfer analysis. Section H-Real gas results via the van der Waals equation of state and viral-expansion extensions of its limiting Abel-Noble form,” Livermore, CA, 1983.

[30] The Engineering ToolBox, “Resources, tools and basic information for engineering and design of technical applications,” 2017. [Online]. Available: http://www.engineeringtoolbox.com/index.html.

[31] M. Kuznetsov, S. Pariset, A. Friedrich, G. Stern, J. Travis, and T. Jordan, “Experimental investigation of non-ideality and non-adiabatic effects under high pressure releases,” *Int. J. Hydrogen Energy*, vol. 40, no. 46, pp. 16398–16407, Dec. 2015.

[32] United Nations Economic Commission for Europe, “Global technical regulation on hydrogen and fuel cell vehicles,” 2013.

[33] D. Makarov, Y. Kim, S. Kashkarov, and V. Molkov, “Thermal protection and fire resistance of high-pressure hydrogen storage,” in *Eight International Seminar on Fire and Explosion Hazards (ISFEH8)*, 2016.

[34] MatWeb Material Property Data, “Overview of materials for High Density Polyethylene (HDPE), Pipe Grade,” 2017. [Online]. Available: http://www.matweb.com/search/DataSheet.aspx?MatGUID=c305addb2e1c4a58a3dece14122acfde. [Accessed: 28-Aug-2017].

[35] J. Hu, J. Chen, S. Sundararaman, K. Chandrashekhara, and W. Chernicoff, “Analysis of composite hydrogen storage cylinders subjected to localized flame impingements,” *Int. J. Hydrogen Energy*, vol. 33, no. 11, pp. 2738–2746, Jun. 2008.